Influence of Tip Wear on Atomic Force Acoustic Microscopy Experiments

Malgorzata Kopycinska-Müller, Roy H. Geiss, Paul Rice, and Donna C. Hurley
Materials Reliability Division, National Institute of Standards and Technology
Boulder, CO 80303-3328 U.S.A.

ABSTRACT

Tip wear and its corresponding change in geometry is a major impediment for quantifying atomic force acoustic microscopy (AFAM). To better understand the process of tip wear and its influence on AFAM measurements of material elastic properties, we have performed a series of experiments and compared tip geometries calculated from experimental data with direct tip visualization in the scanning electron microscope (SEM). Using a sample with known elastic properties, the tip-sample contact stiffnesses for several different cantilevers were determined. Hertz and Derjaguin-Müller-Toporov (DMT) contact-mechanics models were applied to calculate values of the tip radius R from the experimental data. At the same time, values for R before and after each sequence of AFAM measurements were obtained from SEM images. Both methods showed that the tip radius increased with use. However, values of R calculated with the theoretical models varied indeterminately from those obtained from the SEM images. In addition, in some cases analysis of the AFAM measurements suggested a hemispherical tip, while the corresponding SEM images showed that the end of the tip was flat. We also observed other changes in tip shape, such as an increase in the tip width. By combining theoretical models for contact mechanics with visual information on the tip geometry we hope to better understand contact characteristic in AFM-based systems.

INTRODUCTION

The efforts of several groups have focused on the evaluation of elastic properties with dynamic enhancements of AFM [1-4]. Despite individual differences in the techniques, such as excitation amplitudes and the range of frequencies involved, all of these methods rely on Hertz or DMT contact-mechanics models to describe the contact between the tip and the sample [5, 6]. Quantitative measurements depend strongly on the characterization of the tip-sample contact. Quantitative elastic-property values have been obtained with the AFAM technique [3, 4]. Values of the indentation modulus obtained with AFAM methods agree very well with results either obtained by nanoindentation or calculated from elastic constants available in the literature. It was noticed, however, that the best agreement is obtained by use of a reference or calibration sample with elastic properties similar to those of the unknown material (or by use of two reference materials, respectively stiffer and more compliant than the unknown sample). In addition, in order to minimize the influence of tip wear and uncertainties connected with the cantilever spring constant and the AFM force calibration, it is important to perform measurements on the reference sample before and after every measurement of the unknown material [3]. In this paper, we describe our work to better understand the process of tip wear that occurs in AFAM experiments. From these experiments, we hope to simplify the calibration procedure described above and improve the accuracy of quantitative elastic-property measurements with AFAM.

DATA ACQUISITION AND EVALUATION METHODS

Several AFM cantilevers were used to perform a sequence of tests that simulated typical AFAM experiments. The first test of the sequence consisted of three AFAM measurements at relatively low static loads (~0.3-1.5 μN). In the three to five tests that followed, we increased the static load up to ~3-5 μN and the number of measurements up to 40 by the last test. The quantity measured in AFAM experiments is the resonance frequency of a cantilever contacting a sample surface. The details explaining how to calculate the tip-sample contact stiffness k^* from the measured contact resonance frequencies can be found elsewhere [3]. The experimental values of k^* were used to estimate the geometries of the tips and to calculate values for the tip radius R for those tips that were considered hemispherical. We also acquired SEM images of the tips before and after each of the AFAM tests. We used commercial software to determine the curvature of a tip, by adjusting the radius of a circle to match the dimensions of the tip as closely as possible. The tip shape and tip radius values obtained from the SEM images were compared to those calculated from the AFAM data.

To calculate R, we needed the value of the spring constant k_c for each cantilever used in our experiments. The values of k_c were calculated from a standard equation [7] for a vibrating rectangular beam with a trapezoidal cross section. The dimensions of the cantilevers were measured from the SEM images. The values of k_c obtained, together with the deflection δ of the cantilever measured by AFM, were used to calculate the static loads $F_c = k_c\delta$ applied during the AFAM measurements. A sample of fused quartz was used for all of the experiments described here. The indentation modulus M of the fused quartz sample was 68.4 ± 1.7 GPa, as measured by nanoindentation. The value M_t = 165.0 GPa for the (100)-oriented cantilever tip was calculated from the elastic constants of single-crystal silicon [3, 8].

We used the Hertz and DMT contact-mechanics models to estimate the geometry of the AFM tips and to calculate values for R. The Hertz contact model assumes that there are no adhesive forces between the indenting tip and the sample. The tip radius R is given by [6]

$$R_H = k^{*3} / (6 F_c E^{*2}) \,, \tag{1}$$

where E^* is the reduced Young's modulus given by

$$\frac{1}{E^*} = \frac{1}{M_t} + \frac{1}{M_s} \ . \tag{2}$$

Here M_t and M_s are the indentation moduli of the tip and the reference sample, respectively. In the experiments described in this study, we knew the values of M_t and M_s, as described above. Thus, by using Eqs. (1) and (2) we were able to calculate the values of R for each AFAM measurement independently.

As shown below, our data were not entirely consistent with the Hertz theory. Therefore, as a second step, we applied the DMT model to analyze our data. The DMT model takes into account the adhesive forces F_{ad} acting between the tip and the sample surface [5]. Values of R can be determined from the slope of the dependence of k^* on F_c.

$$k^{*3} = 6R_{DMT}E^{*2}(F_c + F_{ad})\,. \tag{3}$$

In cases where k^{*3} increased linearly with F_c, we assumed that the tip had a hemispherical shape and calculated R from the slope of the linear regression fit function. The adhesion force F_{ad} is a constant value that can be associated with the y-intercept of the linear regression fit used to analyze the experimental data.

RESULTS AND DISCUSSION

In this paper we will show only a few representative results from our experiments. Figure 1(a) shows the values of tip radius R_H obtained using the Hertz model [Eq. (1)] from the AFAM measurements of k^* as a function of applied static load F_c. The results in Fig. 1(a) were obtained by using a cantilever with a calculated cantilever constant k_c = 33.7 N/m. As can be seen in Fig. 1(a), the values of R increased from one test to the next. Furthermore, instead of having a constant value, as expected from the Hertz model, R decreased with increasing F_c. This behavior was also observed for other AFM tips used in our experiments. This result could indicate the presence of an offset stiffness ($k^* \neq 0$ for $F_c = 0$) originating either from adhesion forces or a nonspherical (for example, flat-punch) tip geometry. For this reason, we also used the DMT model to analyze the experimental values of k^*. Using Eq. (3), one value of R_{DMT} was obtained from each test in the manner described above. Figure 1(b) compares the values of R_{DMT} to the values of R_{SEM} determined from the SEM images taken between each test. We were not able to obtain R_{DMT} for the first test because the tip broke during the test and the resulting experimental values of k^* did not yield a linear dependence on F_c by use of Eq. (3). Figure 1(b) shows that the tip radius values increased with time, but the values of R_{DMT} were always lower than R_{SEM}.

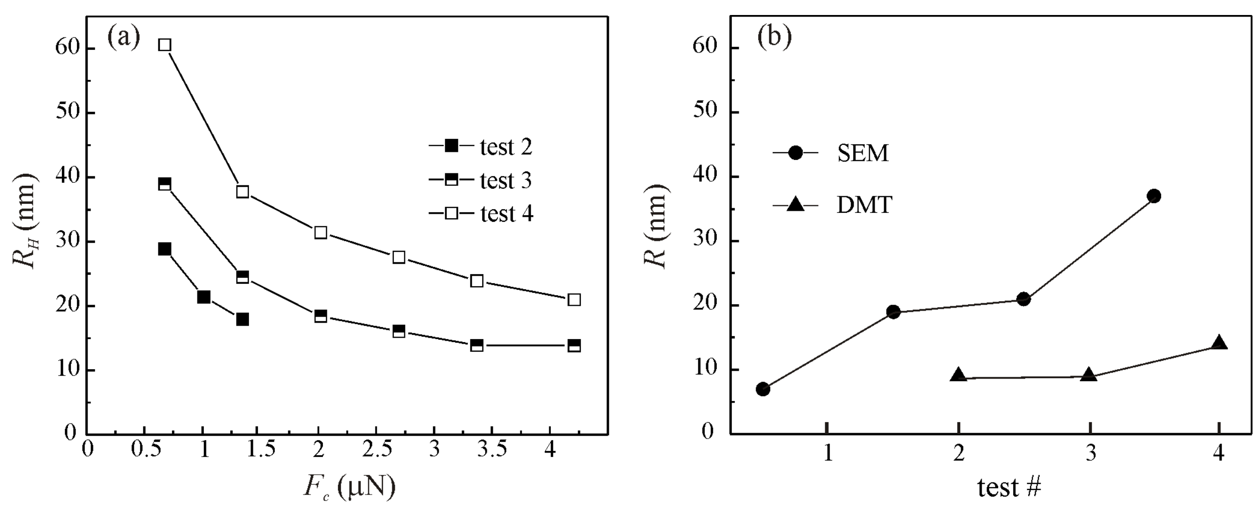

Figure 1. (a) Values for the tip radius R_H calculated from experimental AFAM values of k^* using the Hertz contact model. The estimated uncertainty in F_c is ± 10 %, resulting in an uncertainty of approximately ± 15 % for R_H. (b) Comparison of values for R determined from the SEM images to those obtained from the AFAM data using the DMT contact model.

Figure 2 shows the SEM images that were used to obtain the values of R_{SEM}. The new tip is shown in Fig. 2(a). The tip was very sharp, with R < 10 nm. The SEM image of the tip after the first AFAM measurements, shown in (b), reveals that the tip had broken during measurements. The tip radius has increased significantly (R_{SEM} = 22 nm). The images in Figs. 2 (c) and (d) of the tip after the second and third AFAM tests, respectively, show changes in the tip shape induced during the subsequent AFAM measurements. We also noticed that there are additional changes in the tip shape, for example, a change in tip width as indicated in Figs. 2 (b), (c) and (d). We measured the tip width from the SEM images. We were careful to always measure the width and the same tip height. We concluded that the increase in tip width in this region cannot be explained by tip compression alone. It may be possible that contamination of the tip has occurred.

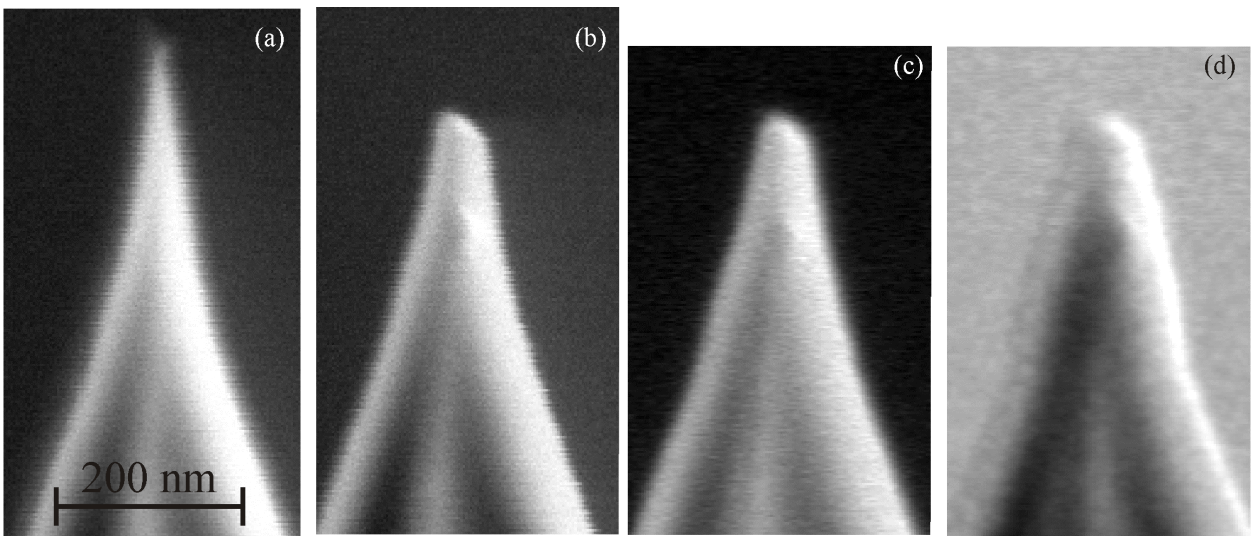

Figure 2. SEM images of an AFM tip. The scale, indicated in (a), is the same for all of the images. (a) New tip with R < 10 nm. (b) Tip after the first AFAM test. The end of the tip has broken off, increasing R. (c) Tip after the second AFAM test. There is little change from (b), consistent with the AFAM results. (d) Tip after third AFAM test. Further increase in R and changes in the tip width can be observed.

The SEM images in Fig. 2 show an AFM tip that can be described as hemispherical, despite wear. However, this is not always the case. Figure 3 shows SEM images of three different AFM tips taken after similar tip wear experiments. Although the actual shape of each one is different, the values of k^* obtained with all of the tips gave a linear dependence on F_c using Eq. (3), suggesting that all of the tips had hemispherical geometry. The shape of the tip in Fig. 3(a) can be described as reasonably spherical. The material indicated by the arrow in the image is probably the remainder of the broken end of the tip. We observed tip fracture during the AFAM measurements with this cantilever. When a tip fractures, its contact resonance frequencies increase significantly from the previous measurement (for instance, by ~70 kHz for the first mode and ~200 kHz for the second mode in this case), yielding much higher values of k^*. The tip in Fig. 3(b) shows an extreme case. This tip was very large (R ~ 50 nm) compared to the other tips, even when new, and its shape was deformed. Based only on the SEM images, it is difficult to determine how much, if any, of the change in tip shape is due to plastic deformation or tip contamination. Figure 3(c) shows another AFM tip after use in AFAM experiments. This tip can be described as a flat punch with R ~ 25 nm. However, the AFAM data obtained with this tip indicated a small hemispherical tip with $R = 13 \pm 3$ nm.

The tips shown in Figs. 2, 3(a) and 3(c) were all very sharp ($R < 10$ nm) initially. All of them fractured during the very first set of AFAM measurements. The way in which they fractured determined the subsequent shape of the tip. However, each of the tips behaved differently. So far, we have not observed a pattern to the behavior that will allow us to predict how the tip will wear and change shape. It should be emphasized that regardless of their geometry or changes in shape, all of the tips provided useful AFAM data (aside from the measurements adjacent to tip fracture).

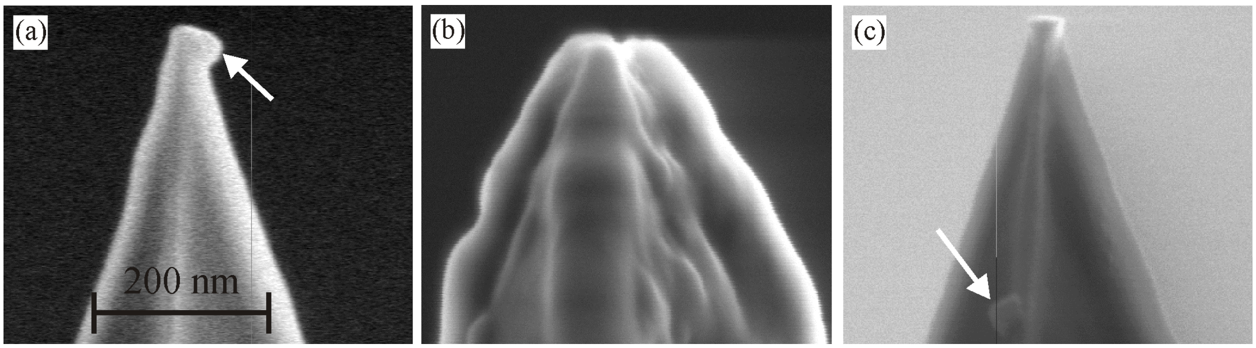

Figure 3. SEM images of three different AFM tips. Despite their dissimilar geometries, all of the tips yielded AFAM data that suggested hemispherical tip shapes. (a) Despite tip fracture, the tip is still relatively sharp and approximately round at the end. (b) The geometry of this tip is complex in comparison to the other tips. The tip shape changed dramatically during the experiments. (c) Example of flat-punch geometry. The arrow shows a particle of an unknown origin that contaminated the tip during the experiments.

The discrepancy between the information deduced from the AFAM data and that obtained from the SEM images leads to the question of whether macroscopic models can be used to accurately describe the contact mechanics in AFM-based systems. The Hertz contact model assumes that the indenter is a sphere, that there are no adhesion forces between the bodies, and that only one of the contacting bodies deforms during indentation. Our SEM images confirm that sometimes the tips are indeed hemispherical. The adhesion forces are usually so small in comparison to the applied forces that they can be neglected. Pull-off forces observed in our experiments were not larger than 0.1 μN, with their influence becoming smaller with higher static loads.

What about the assumption that the tip does not deform? Standard AFM tips are made from silicon, which has an indentation modulus about 7 times lower than that of the diamond tips used in indentation measurements. The estimated sample elastic deformation (*i.e.*, the indentation depth) in an AFM system consists of deformation of both the sample and the silicon tip. However, the Hertz model assumes that the shape of the tip is constant and independent of length of use or load. When a silicon tip indents a sample with similar elastic properties, the tip shape is altered in a way that depends on the relative elastic properties of the sample and the applied static load. The tip deformation occurring during AFAM measurements could explain the observed dependence of R on F_c shown in Fig. 1(a) and the discrepancy between the values of

R_{DMT} and R_{SEM} in Fig. 1(b). It could also explain why current AFAM techniques require the use of a reference sample with elastic properties similar to those of the unknown material. With this approach, the deformation of the tip on the reference sample is similar to that on the unknown material. Thus the function that describes the dependence of the tip shape on the static load is very similar for both systems. In such a case, the ratio of values of k^* measured on the reference and unknown samples will yield an accurate result for M_s. The use of two reference samples with indentation moduli higher and lower than that of the unknown sample also allows us to accurately account for the tip shape when in contact with the unknown sample.

Further insight may be gained from investigations of the tips after use by transmission electron microscopy (TEM). Preliminary TEM studies of AFM tips used in AFAM experiments revealed the presence of dislocations in the tip in certain instances, indicating that the tip had been plastically deformed during use. Future work involving AFAM and high-resolution TEM experiments of the AFM tips analogous to the AFAM-SEM studies described here is planned.

CONCLUSIONS

We have performed a series of experiments to investigate the wear of silicon AFM tips in AFAM measurements. Experimental AFAM data for the contact stiffness k^* were used to calculate the tip radius R for each measurement using both Hertz and DMT contact-mechanics models. The results of this analysis were compared to information about the tip shape obtained from SEM images. Comparison of the AFAM data and the SEM images indicate that the tip shape does not remain constant but instead changes with use. In addition, the results of our experimental data using the Hertz contact model indicate that the tip shape is dependent on the stress field created and thus on the static load and elastic properties of the materials under investigation. In order to expand the applicability of AFAM and to simplify the necessary calibration procedure, we must include the changes in the tip shape in the Hertz contact model. Experiments such as these, in which AFAM-induced changes in the tip shape are directly observed by SEM and compared to the geometry calculated from the AFAM data, will enable us to better understand the limits of the AFAM technique.

REFERENCES

1. F. Dinnelli, M. R. Castell, D. A. Ritchie, N. J. Mason, G. A. D. Briggs, and O. V. Kolosov, *Phil. Mag. A* **80**, 2299 (2000).
2. K. Yamanaka, Y. Maruyama, T. Tsuji, and K. Nakamoto, *Appl. Phys. Lett.* **78**, 1939 (2001).
3. U. Rabe, S. Amelio, M. Kopycinska, S. Hirsekorn, M. Kempf, M. Göcken, and W. Arnold, *Surf. Interface Anal.* **33**, 65 (2002).
4. D. C. Hurley, K. Shen, N. M. Jennett,and J. A. Turner, *J. Appl. Phys.* **94**, 2347 (2003).
5. B. Cappella and G. Dietler, *Surf. Sci. Rep.* **34**, 1 (1999).
6. K. L. Johnson, *Contact Mechanics* (Cambridge University Press, Cambridge UK, 1985), p. 90-96.
7. W. C. Young, and R. G. Budynas, *Roark's formulas for stress and strain* (McGraw-Hill, New York, 2002), p. 189.
8. G. Simmons and H. Wang, *Single crystal elastic constants and calculated aggregate properties: A Handbook* (The MIT Press, Cambridge, MA, 1971), p. 85.